A CROSS-CALIBRATED, MULTIPLATFORM OCEAN SURFACE WIND VELOCITY PRODUCT FOR METEOROLOGICAL AND OCEANOGRAPHIC APPLICATIONS

BY ROBERT ATLAS, ROSS N. HOFFMAN, JOSEPH ARDIZZONE, S. MARK LEIDNER, JUAN CARLOS JUSEM, DEBORAH K. SMITH, AND DANIEL GOMBOS

A consistent 20-yr plus 25-km-resolution ocean surface wind data record is produced using a variational analysis method to combine extensive cross-calibrated multiple satellite datasets with in situ data and ECMWF analyses.

July 1987 marks the beginning of the modern period of remote sensing over the global oceans. Beginning with the launch of the Defense Meteorological Satellite Program (DMSP) *F08* satellite carrying the Special Sensor Microwave Imager (SSM/I), remote sensing coverage of the global oceans every 6 h increased from 20% in 1987 to nearly 70% in 2004. Since 1987, more than a dozen satellite microwave radiometers or scatterometers capable of monitoring the ocean surface wind became operational. Winds at the ocean surface are a key element in the Earth system and critically important to oceanographic and atmospheric applications. Ocean surface winds are crucial to determining fluxes of momentum, energy, and mass between the atmosphere and ocean. These processes include surface stresses that drive ocean circulation and wave generation, sensible heating that warms or cools the boundary layer, evaporation that moistens the atmosphere and increases ocean salinity, and gaseous exchange that transfers CO_2 and other gases between the ocean and the atmosphere. Consistent, high-resolution, time-resolved ocean surface wind datasets are needed to better understand, assess, and predict these processes, as well as to document any changes that occur because of long-term fluctuations, such as El Niño–Southern Oscillation (ENSO), or secular trends, as the climate changes.

Regular, global sampling of the World Ocean is necessary to create the required datasets for these applications. SSM/I, which became operational in 1987, provides an initial capability satisfying this requirement. SSM/I is a microwave radiometer carried by the DMSP series of satellites. SSM/I conically scans Earth's surface from a sun-synchronous near-polar orbit. Wind speeds retrieved from SSM/I are reported

AFFILIATIONS: ATLAS—Atlantic Oceanographic and Meteorological Laboratory, National Oceanic and Atmospheric Administration, Miami, Florida; HOFFMAN, LEIDNER, AND GOMBOS—Atmospheric and Environmental Research, Lexington, Massachusetts; ARDIZZONE AND JUSEM—Goddard Space Flight Center, NASA, Greenbelt, Maryland; SMITH—Remote Sensing Systems, Santa Rosa, California
CORRESPONDING AUTHOR: Robert Atlas, NOAA Atlantic Oceanographic and Meteorological Laboratory, 4301 Rickenbacker Causeway, Miami, FL 33149
E-mail: robert.atlas@noaa.gov

The abstract for this article can be found in this issue, following the table of contents.
DOI:10.1175/2010BAMS2946.1

A supplement to this article is available online (10.1175/2010BAMS2946.2)

In final form 23 July 2010
©2011 American Meteorological Society

every 25 km, with an effective resolution of 37 km and a reported accuracy of 1 m s^{-1} (Wentz et al. 2007). Note that wind direction is retrieved from scatterometers, but most microwave radiometers, including SSM/I, do not yield directional information.

With the exception of Tropical Rainfall Measuring Mission Microwave Imager (TMI), most instruments that provide data used here are in polar orbits with a period of approximately 100 min at an altitude of approximately 800 km and observe a swath of ocean 1,500–1,800 km wide. At the equator, successive orbits are spaced approximately 2,700 km apart, so as much as two-thirds of the equator is observed twice each day, once by ascending and once by descending passes by each satellite. Data coverage between 30°S and 30°N is further enhanced with the inclusion of TMI beginning in 1997. Figure 1 shows the satellite wind speed coverage for a 6-h period in 2004 for a single polar-orbiting satellite and the combined coverage using all available satellite winds. Satellite surface wind data are obtained from Remote Sensing Systems (RSS; Santa Rosa, California; available online at www.remss.com/).

With this wealth of data, our ability to monitor and understand the ocean and air–sea interactions has increased markedly. The purpose of the project described here is to combine these data into a cross-calibrated multiplatform (CCMP), long-term, high-resolution data record of ocean surface winds. With enough sensors, we do get nearly complete coverage each 24-h period, but the data are asynchronous and still incomplete. An important type of data gap is evident in Fig. 1 in the Gulf of Mexico where the SSM/I data are affected by rain associated with Hurricane Ivan and winds cannot be retrieved. All the sensors used here are sensitive to rain, and increasing rain rate is associated with decreased accuracy and data gaps. This results in a sampling bias. Further, some weather features move quickly, and estimates of the ocean surface wind are needed every 6 h to resolve the motions of storms. Data coverage within a 6-h period is far from complete. Typically, at weather forecast centers, all available data, including the ocean surface wind data (in principle but only lately and only partially in practice), are combined with a prior estimate, usually taken to be the most recent 6-h forecast. The resulting analyses provide good estimates of the state of the atmosphere, including the ocean surface winds. Such analyses (or reanalyses) are relatively coarse and tuned to provide good initial conditions for weather forecasts (Kalnay et al. 1997; analysis resolution is effectively controlled by the specification of the background error covariances; e.g., Courtier et al. 1998, Figs. 1–3). We

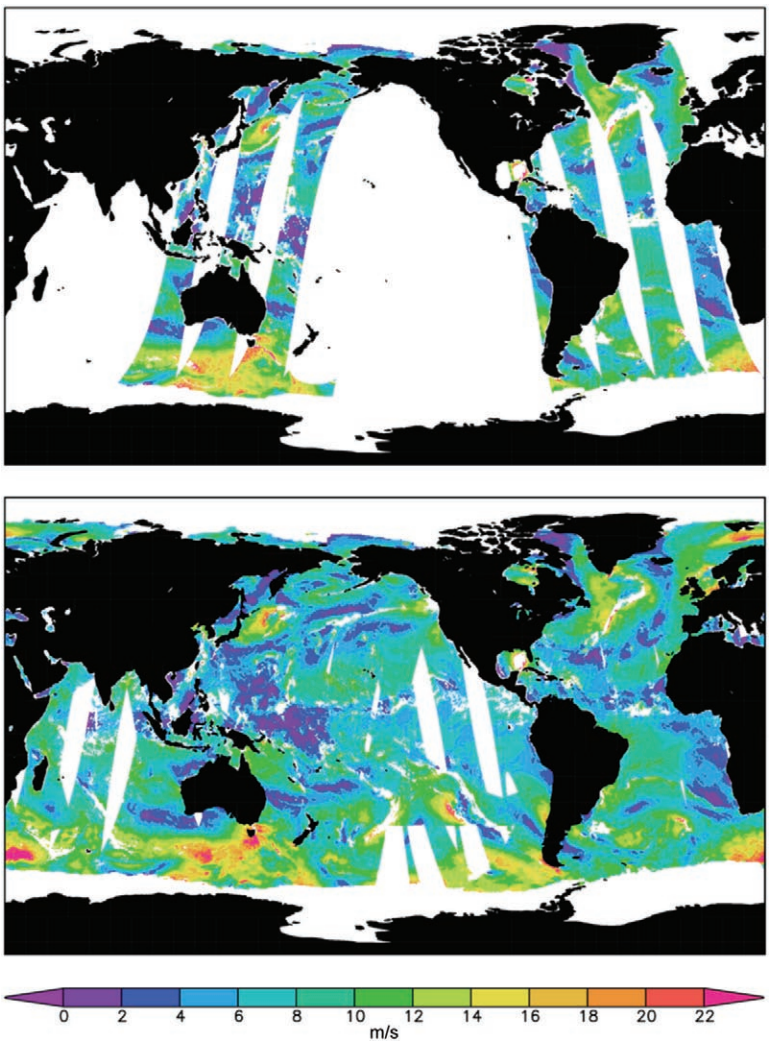

Fig. 1. Satellite surface wind speed coverage for a 6-h period on 14 Sep 2004. Speeds are shown as shaded colors (m s^{-1}). (top) Coverage from a single SSM/I satellite (*F13*). (bottom) The total coverage using the cross-calibrated satellite surface wind datasets from RSS, which include SSM/I (*F13–F15*), AMSR-E, TMI, and QuikSCAT. All satellite surface wind measurements are affected by rain, resulting in data gaps in the coverage. This is clearly evident in the Gulf of Mexico around Hurricane Ivan.

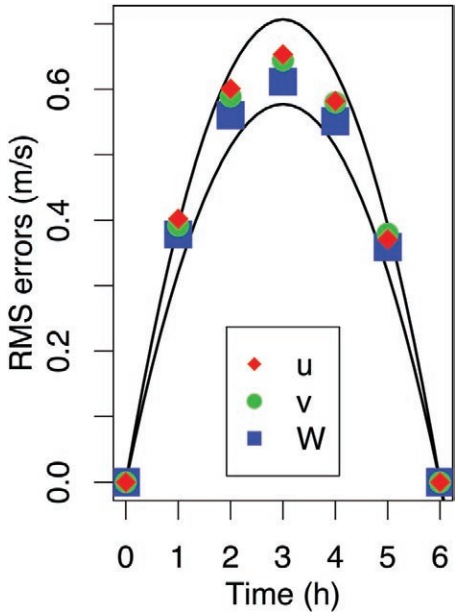

Fig. 2. FGAT errors versus the WRF model-predicted 10-m winds for each hour within a 6-h window. The region of interest is over Typhoon Meranti on 8 Aug 2004. The FGAT algorithm uses linear interpolation of *u* and *v* of the 0- and 6-h wind field.

use analyses and reanalyses from the European Centre for Medium-Range Weather Forecasts (ECMWF) as prior information that we combine with all the satellite data from RSS and available conventional data using a variational analysis method (VAM).

A number of other investigators have created ocean surface wind datasets from satellite data previously. Three different approaches are exemplified by the work of Milliff et al. (1999), Zhang et al. (2006), and Bentamy et al. (2007). Milliff et al. (1999, appendix A) combined Quick Scatterometer (QuikSCAT) and *European Remote Sensing Satellite-1* (*ERS-1*) winds with National Centers for Environmental Prediction (NCEP) analyses using spline interpolation and wavelet reconstruction to fill in high-resolution features between scatterometer swaths. Zhang et al. (2006) combine all the RSS data using Gaussian weights depending on distance and time offset, taking directional information from reanalyses or analyses as needed. Bentamy et al. (2007) describe a real-time high-resolution optimal interpolation method that blends QuikSCAT and SSM/I data with ECMWF analyses over the Mediterranean Sea. Like Zhang et al. we make use of all available RSS data and like Milliff et al. and Bentamy et al. we combine these data with a background field. However, as described below, the VAM can make use of wind speed alone to influence the analysis of wind components.

The purpose of this paper is to describe our methodology (in the methodology section) and datasets (both input and output in the datasets section), to demonstrate consistency and accuracy of our results (in the validation section), and to present selected results and compare to previous investigations (in the patterns of marine surface winds section). Each of these sections is introduced with background material to provide context. We conclude with a summary, discussion, and plan for future improvements (in the conclusions and future plans section).

METHODOLOGY. The VAM best fits all available data while simultaneously satisfying a number of smoothness constraints and a dynamical constraint. The VAM was originally designed to resolve the directional ambiguity of scatterometer wind observations (Hoffman 1982, 1984). Atlas et al. (1996) modified the VAM to assimilate satellite wind speeds and created

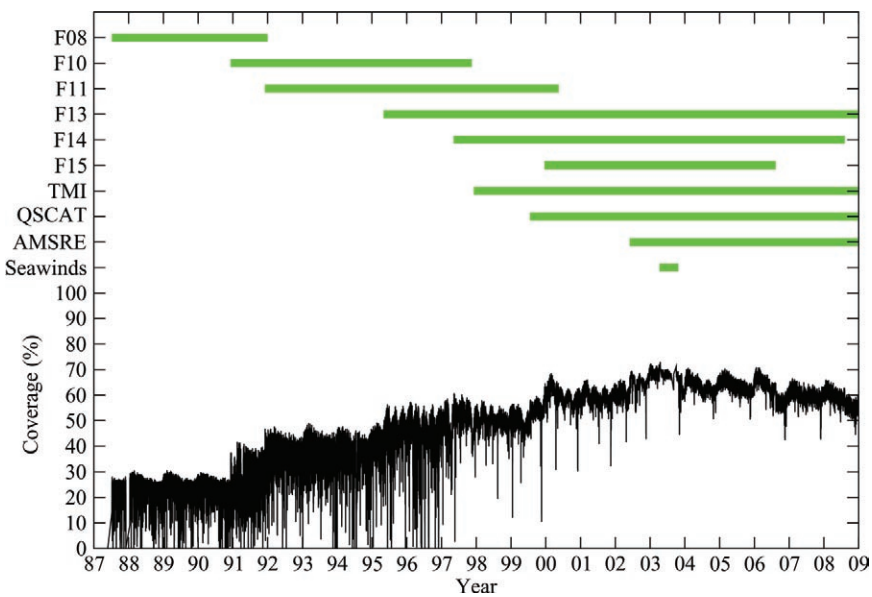

Fig. 3. Time availability of satellite surface wind datasets analyzed by the VAM. The SSM/I instruments are denoted *F08–F15*. The percentage of the global oceans observed by these missions in a 6-h period is shown in the bottom portion of the graph.

THE VAM MULTIPASS QC PROCEDURE

The VAM multipass QC procedure reassesses the quality of the observations as other data are assimilated. This allows data that are initially rejected to be reconsidered as the analysis converges to a final solution. In the multipass procedure, four linked analyses are calculated at increasingly detailed grid resolutions. Using coarser grids during the preliminary passes improves computational efficiency. The first analysis is on a 1° × 1° latitude–longitude grid. The solution on the 1° grid seeds an analysis on the 1/2° × 1/2° grid. Then, the solution on the 1/2° × 1/2° grid seeds the analysis on a 1/4° × 1/4° grid. The first 1/4° × 1/4° analysis seeds a final 1/4° × 1/4° grid. Observation quality is assessed prior to each analysis by comparing each observation to the analysis just completed or, in the case of the first analysis, to the ECMWF background. For each succeeding QC pass, the tests become stricter, but still some data previously rejected may be accepted because the new comparison is to an analysis that may have used neighboring supporting data. The first three analyses are used for QC and to seed the next analysis and therefore make use of a looser convergence criterion than the final analysis, which is identified as the CCMP analysis.

a precursor to the data product described here using SSM/I winds only, first at 2° × 2.5° resolution and then at 1° × 1° resolution. The VAM has also been applied to ambiguity selection for the National Aeronautics and Space Administration (NASA) Scatterometer (NSCAT; Henderson et al. 2003). Here, the VAM is extended to assimilate all satellite surface winds and to preserve small-scale features in the satellite data so that useful 1/4° resolution analyses can be created. In this application, the variational approach is preferred to the simpler statistical (or optimal) interpolation methods because the VAM easily accommodates a nonlinear observation operator, which in this case includes the calculation of wind speed from the analysis u and v wind components. Also the VAM wind directions should be an improvement over simply assigning the ECMWF directions to the radiometer wind speed observations (Atlas et al. 1996, section 2c; Atlas 1997, Fig. 11; see "Comparison to scatterometer winds" in the supplement).

The variational analysis method. The variational analysis (Hoffman et al. 2003) generates a gridded surface wind analysis by minimizing an objective function J:

$$J = \lambda_{\mathrm{CONV}} J_{\mathrm{CONV}} + \lambda_{\mathrm{SCAT}} J_{\mathrm{SCAT}} + \lambda_{\mathrm{SPD}} J_{\mathrm{SPD}} + \lambda_{\mathrm{VWM}} J_{\mathrm{VWM}} + \lambda_{\mathrm{LAP}} J_{\mathrm{LAP}} + \lambda_{\mathrm{DIV}} J_{\mathrm{DIV}} + \lambda_{\mathrm{VOR}} J_{\mathrm{VOR}} + \lambda_{\mathrm{DYN}} J_{\mathrm{DYN}}.$$

Here, J measures the misfit of the analysis from different types of observations ($CONV$ = conventional, $SCAT$ = scatterometer, and SPD = speed), the background (VWM = vector wind magnitude), a priori smoothing constraints (LAP = Laplacian of wind components, DIV = divergence, and VOR = vorticity), and a dynamic constraint (DYN). The CCMP analysis is the final result of a multistage procedure that allows for adaptive quality control (QC; see sidebar on the VAM multipass QC procedure). The λ are weights controlling the amount of influence each constraint has on the final analysis. It should be noted that, although λ symbols are often used to denote Lagrangian multipliers, here the constraints are all weak constraints and the λ are weights. The sidebar on the VAM cost function provides a brief definition of each constraint and our approach to setting the λ weights (for details, see Hoffman et al. 2003). Because we are using selected ambiguities here, each scatterometer observation is treated as a conventional wind observation. Therefore, the form of J_{SCAT} and J_{CONV} are the same. In other work cited, all scatterometer ambiguities or the two principal ambiguities were used and the form of J_{SCAT} is considerably complicated. In previous work (Atlas et al. 1996), we treated SSM/I wind speed data as nadir scatterometer wind speed data. [For the 1978 NASA Sea Satellite (*SeaSat*) scatterometer studied by Hoffman (1982, 1984), observations of speed alone were retrieved in the nadir gap.] Here, J_{SPD} is a microwave ocean surface wind speed observation operator appropriate for SSM/I and similar instruments.

Three significant enhancements made to the VAM for the assimilation of ocean surface winds at high spatial resolution are described now.

First guess at the appropriate time. The ocean surface wind product described here maintains the full 25-km resolution of the cross-calibrated microwave sensor datasets. This is a significant increase in resolution over the previous 100-km SSM/I Pathfinder dataset. As spatial resolution is increased, shorter temporal scales must be resolved more accurately. The VAM was modified to compare the analysis and observations at the observation times. This procedure is referred to as the first guess at the appropriate time (FGAT).

The FGAT procedure was designed to account for the first-order effects of the asynopticity of the ocean surface wind observations. The basic FGAT procedure uses the time-interpolated first guess to define the observation increments but assumes the analysis increments are constant with respect to time. Thus, the difference between the analysis V_a and prior or

background V_b at the observation time t is the same as at the analysis time t_1: that is,

$$V_a(t) - V_b(t) = V_a(t_1) - V_b(t_1).$$

For generality, this is implemented as

$$V_a(t) = \alpha V_a(t_1) + V_\delta(t), \qquad (1)$$

where $\alpha = 1$ is a constant, included to allow for different types of time interpolation, and V_δ depends only on the gridded prior wind estimate at three successive analysis times. Because $V_a(t)$ is only needed to simulate observations, (1) needs only to be evaluated at the observation locations and $V_\delta(t)$ can be precalculated and stored with each observation.

THE VAM COST FUNCTION

Each term in the VAM cost function J is defined in Table SB1 as either a sum or an integral. The observation functions are sums over all observations currently accepted by the QC procedures. The background constraints are numerical integrations over the entire analysis domain. Note that away from the influence of data the integrands of all the background constraints are identically zero. The λ weights were chosen to produce the desired balance of contributions from the background wind field and the satellite observations. For the CCMP products, the λ weights produce fits to the observations that are in fact tighter than the RSS estimates of the observational errors (0.5 m s^{-1} vs 0.7 m s^{-1}). (However, the section on time-interpolation errors explains how observations far from the analysis time are given lower weight.) As a result, CCMP directly reflects observations close to the analysis time and smoothly merges the satellite data swaths into the ECMWF background. In Hoffman et al. (2003), the following λ weights were used for the background constraints:

$$(\lambda_{VWM}, \lambda_{LAP}, \lambda_{DIV}, \lambda_{VOR}, \lambda_{DYN})^T = (1, 1, 4, 1, 16)^T.$$

Through a series of sensitivity tests, Hoffman et al. (2003) demonstrated that the VAM can fit scatterometer winds to within about 1 m s^{-1} RMS for a λ_{SCAT} weight of 16 (see Fig. 5 of Hoffman et al. 2003) on a 1° × 1° latitude–longitude grid. However, for the application here, we are not producing a synoptic analysis suitable as initial conditions for a numerical weather prediction model. Instead, these surface wind analyses border on the mesoscale (1/4°) and should reflect the satellite data more than the background, where satellite data are present. So the background constraint λ weights were determined by a series of sensitivity tests (not shown) on a 1/4° global grid to produce an RMS wind speed fit of about 0.5 m s^{-1}. The result was to reduce the influence of the background, $(\lambda_{VWM}, \lambda_{LAP}, \lambda_{DIV}, \lambda_{VOR}, \lambda_{DYN})^T = (1, 1/4, 1, 1/4, 4)^T$, and to increase the influence of surface wind observations, $(\lambda_{CONV}, \lambda_{SCAT}, \lambda_{SPD})^T = (10, 3, 3)^T$. The sensitivity tests were like those shown in Hoffman et al. (2003). Because of the cross calibration used to produce the satellite observations in this study (see section on Satellite surface winds), it was not necessary to specify different λ weights for individual observing platforms. An RMS fit of 0.5 m s^{-1} is a compromise between direct data insertion (i.e., zero misfit) and traditional blending of observations into a background field for numerical weather prediction (2–4 m s^{-1} RMS). Although it is possible to construct wind fields that more closely fit the satellite observations (e.g., Bentamy et al. 2007), this is generally not possible where data swaths overlap closely in time and is likely to create discontinuities at data swath edges.

Table SB1. Terms in the VAM cost function. Here, V is velocity with components (u,v), ψ and χ are stream function and potential function, and ζ is relative vorticity. Subscripts A, B, and O denote analysis, background, and observation, respectively.

Term	Expression	Description of constraint
		Observation function for the
J_{CONV}	$\Sigma(\mathbf{V}_A - \mathbf{V}_O)^2$	• wind vectors
J_{SCAT}	$\Sigma(\mathbf{V}_A - \mathbf{V}_O)^2$	• wind vectors
J_{SPD}	$\Sigma(\lvert\mathbf{V}_A\rvert - \lvert\mathbf{V}_O\rvert)^2$	• wind speeds
		Background constraints on the
J_{VWM}	$\int (\mathbf{V}_A - \mathbf{V}_B)^2$	• vector wind magnitude
J_{LAP}	$\int [\nabla^2(u_A - u_B)]^2 + \int [\nabla^2(v_A - v_B)]^2$	• Laplacian of the wind components
J_{DIV}	$\int [\nabla^2(\chi_A - \chi_B)]^2$	• divergence
J_{VOR}	$\int [\nabla^2(\psi_A - \psi_B)]^2$	• vorticity
J_{DYN}	$\int (\partial\zeta_A/\partial t - \partial\zeta_B/\partial t)^2$	• vorticity tendency

Time interpolation errors. In areas of overlapping observations from multiple platforms, the linear approximation of the time variation of the wind components inherent in the FGAT procedure can lead to unrealistic analysis increments. Recognizing that data far from the analysis time are less valuable because of the assumption of linear in time variation of the wind components, the FGAT procedure was enhanced to effectively deweight the data as the difference between the observation time and the analysis time increases. To assess the error inherent in the FGAT linear approximation, Weather Research and Forecasting (WRF) model-generated fields were compared with linear estimates from FGAT (Hoffman and Leidner 2010). Differences were plotted at 1-h intervals within a 6-h window for 10-m wind components and speed. Results for these three variables clearly show a parabolic shape that we adopt to parameterize the FGAT error curve (see Fig. 2). For CCMP, we set the magnitude of the 3-h FGAT error equal to the estimated observation error for wind components (1 m s^{-1}). The VAM observation operator (i.e., the contribution to J due to a single observation) for each observation type was adjusted to include this effect through the effective observation error standard deviation, assuming that instrumental and time interpolation errors are uncorrelated.

Updated dynamical constraint. The constraint that requires that the time rate of change of the vorticity of the analysis be small may not apply at high spatial resolution. We reformulated the dynamical constraint to be the integral of the squared difference between the analysis and background time rate of change of vorticity at the surface (Table SB1). This avoids damping or eliminating small-scale features in the analysis where the time rate of change of vorticity might be large.

DATASETS. The amount and quality of ocean surface wind data and analyses based on these data have improved markedly over the last several decades. Conventional observations are few in number, are often poor in quality, and have a spatial sampling pattern restricted by routes of the ships of the voluntary observing program and the difficulty of servicing buoys in remote locations. Recently, however, modern buoys with improved accuracy have been deployed in special observing programs. Data from these buoys are an invaluable ground truth dataset. Beginning in the 1970s, a number of experimental satellite sensors demonstrated that the roughening of the ocean surface by the wind provides a mechanism for the microwave remote sensing of the ocean surface wind from space. The active sensing of the radar backscatter of centimeter-scale capillary waves allows the retrieval of ocean surface wind vectors by scatterometers, albeit with some directional ambiguity. Passive microwave remote sensing of the ocean surface also has the capability of retrieving ocean surface wind speed through the response of the microwave emissivity to the surface roughness (Wentz et al. 1986). The major limitation of such data has been the lack of wind directions; however, new advanced microwave radiometers such as the Navy WindSat Coriolis instrument (referred to simply as WindSat) measure polarization of the microwave radiation, thereby allowing retrieval of some wind direction information (see comparison to WindSat winds section). As will be seen below, the amount of ocean surface wind data has grown tremendously (see also Zhang et al. 2006). Finally, analysis and data assimilation methods have advanced substantially and, as a result, the resolution and accuracy of the resulting products have also improved. Further details about the characteristics and quality of the instruments, the ocean surface winds retrieved, and the associated quality-control procedures are described by Hoffman and Leidner (2005) for scatterometers (specifically QuikSCAT) and by Hollinger et al. (1990) and Wentz (1997) for microwave radiometers (specifically SSM/I).

Satellite surface winds. Data from three types of microwave radiometer sensors were used by RSS to generate cross-calibrated wind speeds. These sensors are the SSM/I, the TMI, and the Advanced Microwave Scanning Radiometer for Earth Observing System (AMSR-E). Two scatterometers of the same NASA design, called SeaWinds—one on the second Japanese Advanced Earth Observing Satellite (*ADEOS-2*; i.e., the *Midori-2* satellite) and one on the NASA QuikSCAT satellite—were used by RSS to generate cross-calibrated wind speeds and directions. We will refer to these two scatterometers as SeaWinds and QuikSCAT, respectively. The scatterometer wind direction information is important for improving the quality of the VAM analyses. Figure 3 shows the availability of satellite ocean surface wind products from RSS. As noted above, measurements from both microwave radiometers and scatterometers are more closely related to ocean surface roughness and hence to wind stress than to the actual wind. For this reason, retrieved winds are reported as the equivalent neutral stability winds at a height of 10 m.

The cross-calibrated microwave radiometer wind speeds are retrieved as part of the RSS simultaneous

retrieval of temperature, surface wind speed, columnar water vapor, columnar cloud water, and surface rain rate. This retrieval method, called the unified microwave ocean retrieval algorithm (UMORA), is based on the fundamental principles of radiative transfer as described by Wentz and Spencer (1998) and updated as described by Hilburn and Wentz (2008). RSS uses an accurate sea surface emissivity model (Meissner and Wentz 2004) and has rigorously (i) intercalibrated the microwave radiometer brightness temperatures, (ii) intercalibrated the QuikSCAT and SeaWinds scatterometer wind speeds to the microwave radiometer wind speeds, and (iii) validated all the satellite winds obtained by comparing to buoy winds. This results in much better consistency for wind speed retrievals across this suite of instruments. According to Hilburn and Wentz (2008), intercalibration errors are 0.1–0.2 K or less across the suite of microwave radiometers and within 0.1 K for the SSM/I series of instruments. QuikSCAT wind directions have been compared to those from moored buoy data for a 10-yr period (1999–2009), providing over 350,000 collocations. The overall direction bias is near 1.5°, and the standard deviation of the difference is 14.8° when ~1% of the data have been edited to remove gross ambiguity selection errors. The standard deviations of the difference increases to over 20° for wind speeds of <4 or >25 m s^{-1}.

Ocean vector winds are obtained from QuikSCAT and SeaWinds scatterometers using the Ku-2001 model function (Wentz and Smith 1999; Wentz et al. 2001, 2003). These winds extend from 0 to 50 m s^{-1} and are of excellent quality except when rain is present. Two rain flags (one developed using the scatterometer and one containing collocated radiometer rain data) are used to remove rain-affected winds from the CCMP product. Validation of RSS scatterometer wind speeds show a 1 m s^{-1} standard deviation with respect to moored ocean buoys (Wentz et al. 2005). The standard deviation is lower (<0.75 m s^{-1}) for high-quality tropical buoys such as those in the Tropical Atmosphere Ocean (TAO) or Prediction and Research Moored Array in the Tropical Atlantic (PIRATA) arrays described below.

Conventional winds. The conventional data used in our analyses are obtained from the National Center for Atmospheric Research (NCAR). These consist of all ship and buoy observations of surface wind. In addition to the standard observations, additional buoy data are obtained from the Pacific Marine and Environmental Laboratory (PMEL) TAO project (McPhaden et al. 1998, appendix B). These data consist of moored ocean buoys for improved detection, understanding, and prediction of El Niño and La Niña. When available, buoys from PIRATA (Bourlès et al. 2009) are also used. Please note that the availability of some of the buoy data from the TAO and PIRATA arrays is contingent on cruise schedules. Conventional wind data are adjusted to 10-m height as described in the supplement (see section on height adjustment for wind observations). No other changes are made to conventional data, and provided QC flags are used to eliminate suspect data.

Background winds. The VAM requires a background (or first-guess) analysis of gridded u and v wind components as a prior estimate of the wind field. For this project, two datasets were used as the prior wind field. For the period July 1987–December 1998, 10-m winds from the 40-yr ECMWF Re-Analysis (ERA-40) were used as a background. During this period the reanalysis has better forecast skill than the operational analyses that were made in real time. However, beginning in 1999, with the benefits of four-dimensional variational data assimilation (4DVAR) and increased spatial resolution, the ECMWF operational (ECOP) analysis outperforms the ERA-40 (Uppala et al. 2005) and is used here for the background.

Distributed products. VAM-assimilated products are produced when all input datasets become available, including the ECMWF background wind fields and the cross-calibrated ocean surface wind datasets from RSS. The CCMP product contains three standard datasets. The primary dataset, denoted as level 3.0, contains 6-hourly gridded VAM analyses. The two other levels of data processing are denoted as levels 2.5 and 3.5. The level-2.5 datasets, one for each passive microwave sensor, are obtained by assigning directions from the VAM analyses (interpolated to the observation time and location) to the input wind speed observations. The level-3.5 datasets are obtained by averaging the level-3.0 dataset over 5-day and monthly periods. Table 1 summarizes each dataset in the CCMP wind product. All datasets are provided on the RSS 1/4° latitude–longitude grid. The latitude extent for the TMI level-2.5 datasets is limited by the low orbital inclination of the spacecraft.

Two versions of the level-3.5 data are produced. For level 3.5A, only those grid points with one or more analyzed observations are used in the average to ensure that the time means represent the satellite-sampled climatology. For level 3.5B, all grid points are used in the average. Because the level-3.5 data are meant to be time averages, both cases use a

Table 1. The CCMP product description. Three dataset types are included in each product release: levels 3.0, 3.5, and 2.5. All these data are presented on a 1/4° latitude–longitude grid. Please note that level-2.5 datasets are stored in a format that is consistent with the original dataset retrieved from RSS. Wind components for QuikSCAT and SeaWinds scatterometers analogous to the level-2.5 data described here are available at the RSS Web site (available online at www.remss.com). The variables in the table are as follows: *u* is the *u* component of wind (m s^{-1}); *v* is the *v* component of wind (m s^{-1}); *W* is the wind speed (m s^{-1}); u_* is the *u* component of pseudostress (m^2 s^{-2}); v_* is the *v* component of pseudostress (m^2 s^{-2}); N_o is the number of observations used in the VAM analysis; and N_t is the number of times averaged.

Dataset	Level	Lat extent (degrees)	Time frequency	Content
Analyses	3.0	78.375	6-hourly	u, v, N_o
Monthly means	3.5	78.375	monthly	u, v, W, u_*, v_*, N_t
Pentads	3.5	78.375	5-day	
SSM/I, AMSR-E	2.5	78.375	daily	u, v
TMI	2.5	39.875	daily	

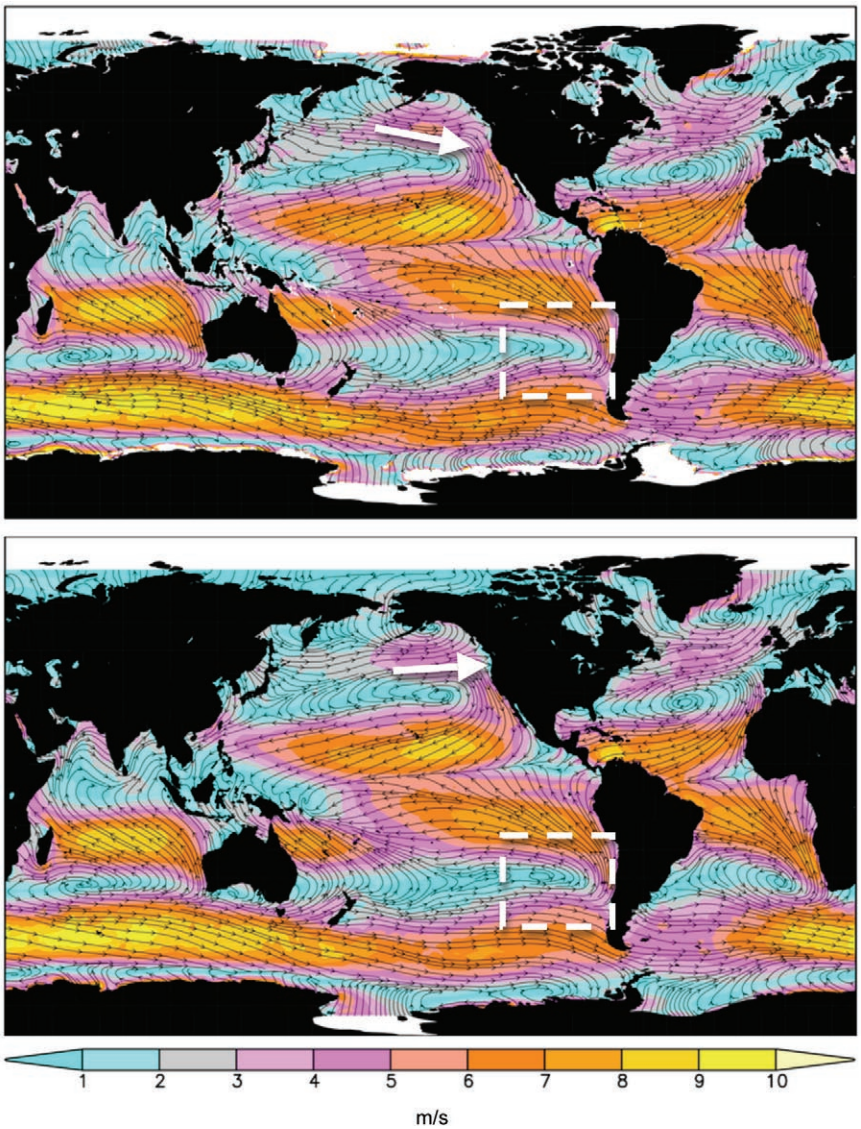

simple average, not an average weighted by estimated accuracy. For most applications, the level-3.5B data are preferred. As mentioned earlier, microwave sensors cannot reliably retrieve ocean surface winds in the presence of rain. This introduces a fair weather bias in satellite-only-derived time-averaged wind fields. Figure 4 demonstrates this by comparing the 2006

Fig. 4. Annual-mean streamlines and vector magnitude (2006) using (top) level 3.5A and (bottom) level 3.5B. Satellite-only-derived climatologies do not accurately represent poleward winds around cyclones where rain is likely to be present. Anticyclonic circulation centers associated with the Hadley cell are less pronounced in the satellite-sampled climatology, as can be seen for example in the boxed region. (top) There is also an overall equatorward trend in the satellite-sampled time average, as is evident in the turning of the mean wind just south of Alaska (see arrow).

Table 2. Analysis products compared to assimilated observations. Wind speed, vector wind, and wind direction difference statistics are in m s^{-1}, m s^{-1}, and degrees, respectively. Values given are representative, but noticeable temporal variability and trends can be found in some cases as described in the supplement. A negative mean speed difference indicates the analysis wind speeds are less than observed. A positive mean direction difference indicates that the observed winds are more directed toward low pressure than in the analysis.

Analysis/ reanalysis	Description	Satellite wind speed		QuikSCAT winds		Conventional ship observations			
		RMS speed	Mean speed	RMS vector	Mean direction	RMS speed	Mean speed	RMS direction	Mean direction
CCMP	VAM analysis using cross-calibrated satellite datasets from RSS, including SSM/I, AMSR-E, TMI, SeaWinds, and QuikSCAT	0.5	~0	0.8	~0	1.6	–0.3	11	0.6
SSMP	VAM analysis using RSS version-4 SSM/I datasets only (see Atlas et al. 1996)	1.0	–0.2	2.0	2.0	2.0	–0.5	14	1.0
ERA-40	ERA-40 used as the background for the CCMP analysis until 1998	1.7	–0.5	2.5	2.0	2.2	–0.8	19	1.1
ECOP	ECOP analyses used as background for the CCMP analysis from 1999	1.5	–0.5	2.0	2.0	2.4	–1.0	18	2.1
NCEP–NCAR	NCEP–NCAR first global reanalysis that used the 1995 NCEP operational data assimilation system at T62 resolution.	2.2	–0.5	3.2	–0.5	2.8	–0.9	27	–0.1

annual mean of the level-3.5A and level-3.5B datasets. The two plots are processed identically, except that in the top plot each VAM analysis is masked by the presence of satellite observations that passed quality control. Comparison of these two plots reveals significant differences in the depiction of the general circulation pattern. Anticyclonic circulation centers associated with the Hadley cell are less pronounced in the satellite-sampled climatology as can be seen, for example, in the boxed region. There is also an overall equatorward trend in the satellite-sampled time average as is evident in the turning of the mean wind just south of Alaska. This can be explained by the overall reduction in cyclonic winds due to rain masking as is apparent for Hurricane Ivan in Fig. 1. The elimination of poleward winds associated with cyclones (and the overall reduction in cyclonic vorticity) creates the equatorward bias that we see in the satellite-sampled climatology and can misrepresent the overall general circulation. Reducing the cyclonic vorticity poleward of the descending branch of the Hadley cell results in a weaker gradient of vorticity, so much so that in the bottom panel of the figure the anticyclonic circulation west of South America no longer has a closed circulation center.

VALIDATION. To validate the VAM and estimate the accuracy of the generated CCMP wind fields, the VAM analyzed winds were compared to the assimilated observations including ships, buoys, and satellite winds and to withheld WindSat observations (i.e., to observations from another microwave radiometer that were not used). To show that the CCMP analyses capture the small scales present in the satellite data, we compare spatial Fourier spectra of the satellite data to that of the CCMP and other analyses in the sidebar on comparison of spatial spectra.

Comparison to assimilated observations. Collocation statistics for five analysis datasets are summarized here and in Table 2. The collocation procedure and detailed statistical results as a function of time over the course of the data record for the assimilated observations are given and discussed in the supplement.

The CCMP analysis is nearly unbiased relative to the assimilated wind speeds with an RMS fit of approximately 0.5 m s^{-1}. The SSM/I multiplatform (SSMP; see Table 2 for definition) analysis has a slight negative bias with an RMS fit of approximately 1 m s^{-1}. The NCEP, ERA-40, and ECOP analyses all have larger RMS differences relative to the observations as well as significant low wind speed biases on the order of 0.5 m s^{-1}. However, these analyses include the effects of stability, which can account for approximately 0.2 m s^{-1} of the low bias relative to the neutral RSS winds (Chelton and Freilich 2005).

The CCMP analysis has an RMS vector difference of approximately 0.8 m s^{-1} to the assimilated QuikSCAT data and no directional bias. The RMS fit of the ECOP analysis improves from 2.5 to 2 m s^{-1} in 2002 when ECMWF began to assimilate QuikSCAT data (see supplement). The SSMP analysis, which used the ECOP winds as a background starting in 1994, did not assimilate QuikSCAT and is unable to improve the fit to the QuikSCAT data using speed-only measurements from SSM/I. Both the ERA-40 and ECOP analyses have a directional bias of approximately 2° versus QuikSCAT, whereas the NCEP reanalysis has a small negative directional bias.

COMPARISON OF SPATIAL SPECTRA

We calculated power spectral density of wind speed for SSM/I observations, ECMWF operational (ECOP) analyses, and CCMP analyses and of the differences SSM/I – ECOP, CCMP – ECOP, and SSM/I – CCMP. Figure SB1 displays the mean power spectra for the differences (bold lines), as well as the 75th and 25th quantiles (thin lines), determined independently at each wavenumber. Note that Fig. SB1 is plotted to preserve variance (Emery and Thomson 2001, section 5.6.3.4), with wavenumber times power spectral density plotted versus the log of wavenumber, so that the area under the curve is proportional to the variance associated with that range of wavelengths. For this calculation, ECOP and CCMP analyses were interpolated linearly in space and time to the SSM/I observation locations. Because we use SSM/I as a standard, we only consider wind speed in this analysis. A total of 10 swath segments of length ~ 6,000 km were processed for 22 Jul 2001, and an additional 6 swath segments were processed for 20 Jan 2001. SSM/I locations with missing wind retrievals were filled in with ECOP values. The mean power spectra in Fig. SB1 show that the CCMP analyses fit the SSM/I data well, particularly at long wavelengths. CCMP fits the SSM/I observations better than ECOP fits the SSM/I observations at all scales greater than 150 km; this is increasingly true for increasing wavelength scales above 150 km. The spectral variability, as portrayed by the interquartile range (i.e., the difference between the 75th and 25th quantiles), is highly sensitive to the wavelength scales. At wavelengths greater than 600 km, the variability is quite large for the CCMP, ECOP, and SSM/I winds (not shown) and SSM/I – ECOP and CCMP – ECOP differences but not for the SSM/I – CCMP difference. Because the distributions of the power spectra for the SSM/I – CCMP difference are similar at large wavelengths on a case by case basis, we may conclude that CCMP fits the SSM/I spatial variability uniformly well at these wavelengths. At smaller scales, the power spectra variabilities of SSM/I – ECOP and SSM/I – CCMP are substantial, whereas the small-scale CCMP – ECOP difference spectra are uniformly close to zero; the apparent lack of variability at the power scales of Fig. SB1 for the CCMP – ECOP distribution is consistent with there being approximately no power in the CCMP and ECOP spectra for scales smaller than 200 km (not shown). Also note that because power is nonnegative, the distribution of power is highly positively skewed, resulting in the mean power being much closer to the 75th percentile than to the 25th percentile.

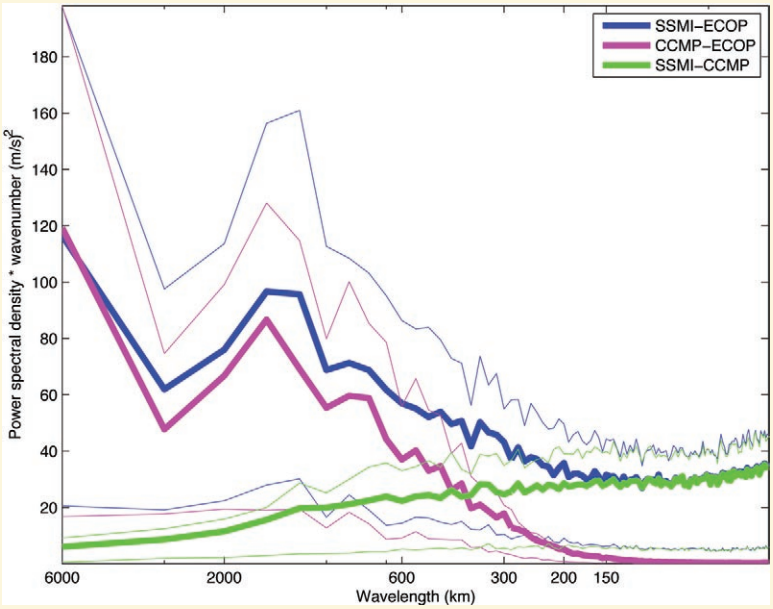

Fig. SB1. Power spectrum of wind speed differences along SSM/I *F15* tracks for SSM/I, CCMP, and ECOP. The mean and 25th and 75th percentile of 1,024 power spectra are plotted at each wavenumber. Units for the y axis are m^2 s^{-2}. The x axis is in units of log of wavenumber, but it is annotated in terms of the associated wavelength (km).

Comparison with conventional (in situ) observations was performed over the year 2001. The last four columns of Table 2 summarize just the results for ships. See the supplement for results for the TAO and other buoys. The CCMP analysis has the best overall fit to the in situ observations with an RMS speed difference ranging from 1.6 m s^{-1} versus ships to 0.6 m s^{-1} versus the higher-quality TAO buoys. This is also seen in the RMS direction fit, which ranges from 11.5° to 7.0°. Overall, the CCMP analysis has a slight negative speed bias on the order of 0.2 m s^{-1} with a negligible direction bias. The directional bias versus ships is consistent with results found versus QuikSCAT observations indicating that the ECMWF analyses are less convergent (more geostrophic) than the VAM analyses that fit the observations more closely.

Comparison to WindSat winds. The Navy WindSat sensor is an advanced polarimetric microwave radiometer launched in January 2003 designed to measure ocean surface wind speed and direction, as well as sea surface temperature, total precipitable water, integrated cloud liquid water, and rain rate over the ocean (Gaiser 2004; Smith 2006). WindSat ocean surface wind directions are not of uniformly high quality, so we compare only wind speeds between WindSat and the CCMP and ECMWF winds. Because the WindSat data were not used in any of the analyses, these are independent data. RMS wind speed differences versus WindSat for a 2-month period in 2004 were found to be 1.0 m s^{-1} for CCMP analyses and 1.6 m s^{-1} for ECOP analyses.

PATTERNS OF MARINE SURFACE WINDS.

The CCMP wind analyses can be significantly different from conventional analysis and reanalysis products from numerical weather prediction centers. The CCMP winds are significantly different in some synoptic cases, result in different storm statistics, and provide enhanced high-spatial resolution time averages of ocean surface wind. More specifically,

- In individual synoptic cases, for example, the CCMP winds sometimes depict storms in different locations or reveal entirely new closed wind circulations.
- With respect to storm statistics, the net impact of assimilating satellite surface winds in the VAM is generally to increase the maximum vorticity and wind speed.
- As an example of the use of CCMP time-averaged datasets, tropical streamline analyses of the monthly averaged VAM analyses reveal the evolution of the El Niño–Southern Oscillation in high spatial definition.
- In addition, patterns in the wind speed difference between the CCMP winds and ECMWF backgrounds often reveal the effects of boundary layer stability and strong ocean currents. Patterns of boundary layer stability are present in these differences because the microwave-derived winds are equivalent neutral stability winds, whereas the background winds are analyzed winds that include stability effects. Signatures of ocean currents are present because the microwave-derived winds are relative to the moving ocean surface, whereas the background winds are not.

CCMP winds also reveal many interesting features of the ocean surface wind field that have been described in greater detail in previous studies of satellite wind observations. These include gap winds (Chelton et al. 2000a,b), island shadows (or wakes), and other phenomena (Chelton et al. 2004).

Storms at sea. Rapidly developing cyclones over the oceans are often difficult to forecast, leaving mariners at great risk for loss of life and cargo. During the 1980s and 1990s, it is estimated that two ships were lost every week on average. Severe weather sank more than 200 supertankers and container ships exceeding 200 m in length. The CCMP winds reveal that the intensity of cyclones over the oceans is often underestimated.

One reason for this is that the CCMP winds better represent and locate storms that are too weak or missing in the background wind field. Figure 5 shows a case study of a cyclone in the North Pacific demonstrating this impact. The background analysis depicts a single cyclone just south of the Kamchatka Peninsula. The VAM analysis reveals a second, more intense cyclone to the south that is consistent with the QuikSCAT winds available to CCMP. The CCMP winds are 15% stronger here than the ECMWF analysis. Moderate Resolution Imaging Spectroradiometer (MODIS) cloud imagery (Fig. 6) confirms the existence of this second cyclone.

Cyclone statistics. Cyclone statistics were computed for January and July 2001 using tracking software to locate and match cyclones in the VAM analysis with the corresponding cyclones in the ECMWF analysis. Once located, maximum vorticity and wind speed within the radius of cyclonic winds are computed. Figure 7 shows the results of this comparison

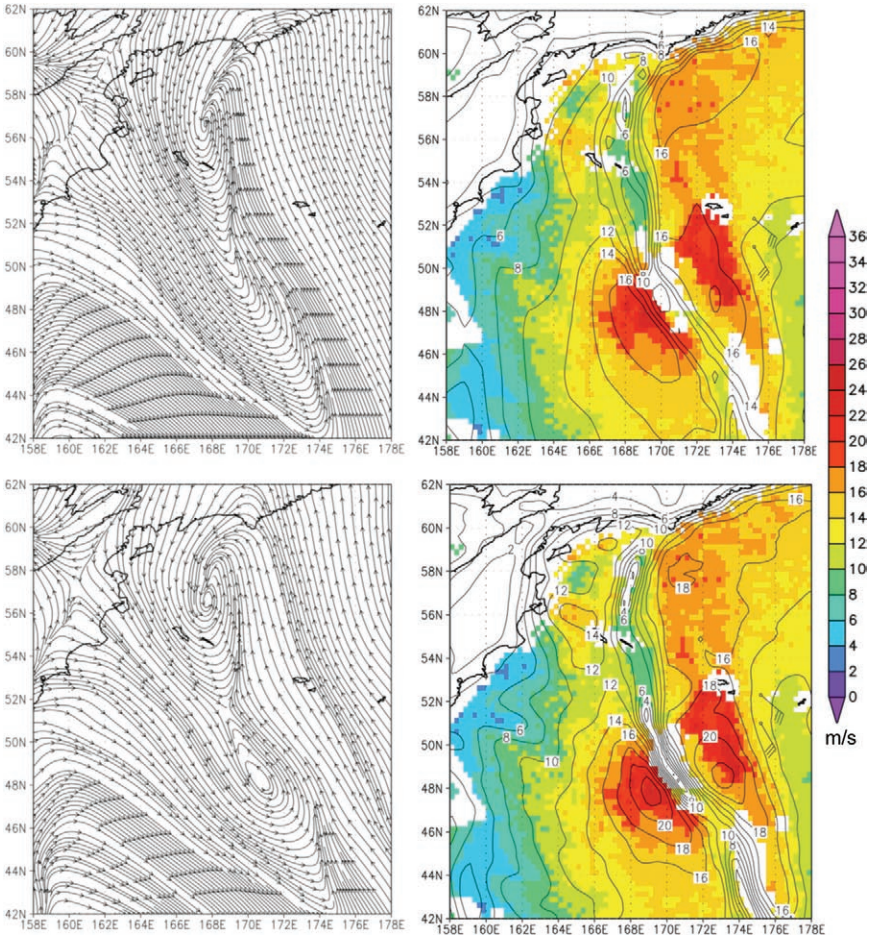

Fig. 5. The 10-m streamlines and wind speed contours for (top) ECMWF and (bottom) CCMP analyses at 0600 UTC 2 Jan 2004 in the North Pacific. The ECMWF analysis depicts a cyclone just south of the Kamchatka Peninsula. The CCMP analysis depicts a second, more intense cyclone to the south. This is consistent with the satellite speeds (shown as shaded colors) depicting a more intense cyclone. Conventional reports (shown as black wind barbs) are also consistent with the satellite-derived speeds.

for various oceanic regions. The net impact of assimilating RSS winds in the VAM is to increase the maximum vorticity and wind speed. The impacts are greatest for winter in each hemisphere. For example, wind speed is increased in storms by about 2 m s^{-1} globally but 3 m s^{-1} or more for Northern Hemisphere winter and 2.5 m s^{-1} or more for Southern Hemisphere winter (Fig. 7b). Similar results hold for vorticity. Although 2 m s^{-1} is small compared to typical storm wind speeds, such changes correspond to large increases in destructive power and substantial increases in air–sea fluxes. Figure 7a shows that vorticity impacts are large and on the same order of magnitude as planetary vorticity.

ENSO monitoring. With 21 yr of data, the CCMP dataset can establish rough measures of the interannual trends in the satellite winds. For example, we will show that ENSO monitoring with satellite surface wind data is possible because of the almost perfect correlation between the surface wind around the dateline and the SST anomalies in the eastern equatorial Pacific. Strengthening (weakening) of easterlies in the central Pacific is accompanied by ENSO cooling (warming) episodes. This relationship is quantified by correlating zonal wind with SST time series from two independent datasets over two different but representative domains. Further, a clear convergent feature in the surface winds marks the surface location of the upward branch of the Walker circulation and provides a simple, data-based visualization of the evolution of ENSO, except in the cold phase.

Figure 8 displays time series of yearly averaged SST in the eastern Pacific and zonal wind in the central Pacific. Each time series is for a standardized anomaly and the annual averages are from July to June and referenced by the ending year. The SST variable is the Oceanic Niño Index (ONI) derived at the National Oceanic and Atmospheric Administration (NOAA; available online at www.cpc.ncep.noaa.gov/products/analysis_monitoring/ensostuff/ensoyears.shtml). ONI is the mean monthly SST anomaly averaged over the Niño-3.4 region (5°S–5°N, 170°–120°W) in the eastern Pacific. The wind variable is the average zonal 10-m wind over the Niño-4 region (5°S–5°N, 160°E–150°W) in the central Pacific. When the CCMP 3.5A dataset is used for the winds, the correlation coefficient between SST and winds is 0.93, confirming the anticipated quasi-perfect linear relationship between these variables. Physically, cold ENSO episodes are accompanied by strong easterlies, whereas warm episodes correspond to weak easterlies around the

dateline. Time series for winds from CCMP 3.5A, CCMP 3.5B, ECOP, and ERA-40 are all very similar at these time and space scales.

Figure 9 shows the annual average streamline and vector magnitude patterns for the western tropical Pacific for each of the 21 years. The Niño-4 region is shown as a white rectangle on each panel. Inspection of these panels reveals the interannual variation of the strength of the easterlies over the Niño-4 region. In addition, a synoptic-scale convergent system (marked by the letter C in Fig. 9) is also evident, except during years of significant cooling. When more than one feature appears on a panel, only the leading one is marked with a C. This feature is a key component of the ENSO cycle marking the surface location of the rising branch of the Walker circulation and following the center of the west tropical Pacific warm pool in a manner that is consistent with the analytic model of the heat-induced tropical circulation of Gill (1980). When a transition to a cold ENSO episode occurs, the convergent feature propagates westward to New Guinea as the intensity of the equatorial easterlies increases in the Niño-4 region. This feature disappears when La Niña is well established as is evident during the years 1989, 1996, 1999–2001, 2006, and 2008 (years of significant cooling in Fig. 8). In contrast, the convergent feature re-forms and propagates eastward as the equatorial easterlies weaken during warm ENSO transitions. One exception to this rule occurs in 1988, where coverage from a single SSM/I satellite (*F08*) is insufficient to represent the annual-mean wind pattern.

Air–sea interaction. Monthly means of the difference between the VAM and ECMWF analyses reveal many phenomena over the oceans. Figure 10a shows the monthly-mean wind speed difference for July 2005. For each grid point, the monthly mean in this case is the average over all synoptic times when satellite data were present at the grid point or at an adjacent or diagonally neighboring grid point. As stated earlier, the ECMWF wind speeds are lower than the CCMP wind speeds by approximately 0.5 m s^{-1}. There are substantial geographic variations in the mean wind speed differences, and examination of patterns in the wind speed difference reveals many interesting features. Some of these differences can be attributed to the nature of the indirect satellite measurement, whereas other features reveal small-scale wind patterns not captured at the coarser resolution of the global analyses. As mentioned above, because wind speeds retrieved from satellites are relative to ocean currents but winds from global analyses are measured relative to the solid Earth, patterns in the wind speed difference between CCMP winds and global analyses often reveal strong ocean currents. Some prominent ocean current features can be seen in Fig. 10a, including the Agulhas Return Current in the South Indian Ocean, the Gulf Stream in the North Atlantic, and the Malvinas Current flowing northward along the continental shelf of Argentina. These ocean currents are also associated with sea surface temperature fronts, which influence the stability

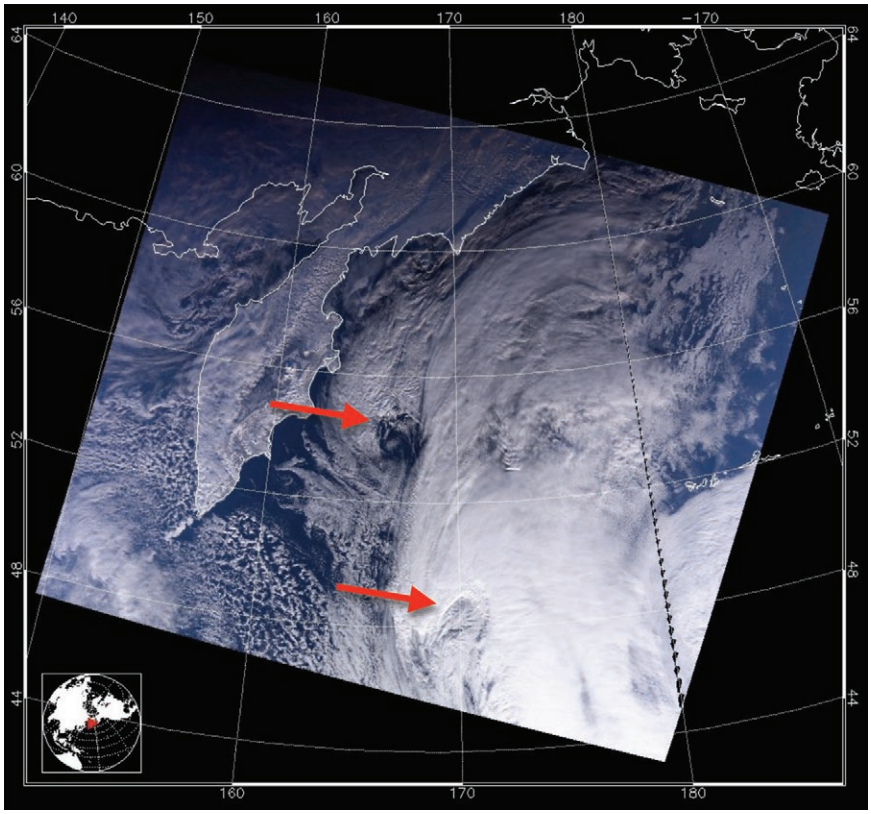

Fig. 6. MODIS cloud imagery for 2 Jan 2004. The arrows indicate the location of two cyclone centers that are clearly evident in the cloud imagery. MODIS imagery was obtained courtesy of NASA (available online at http://modis-atmos.gsfc.nasa.gov).

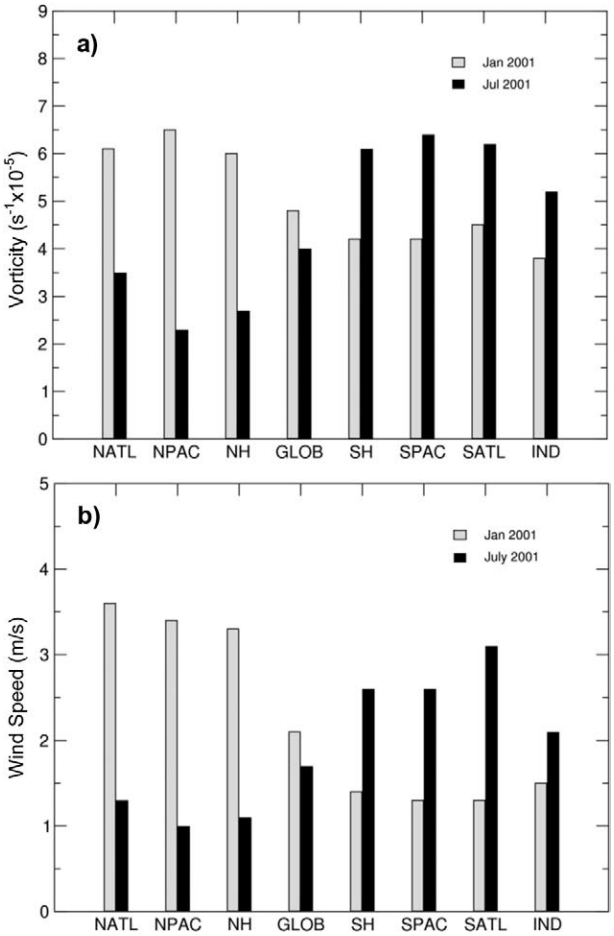

Fig. 7. Cyclone statistics comparing the intensity of cyclones (CCMP − ECOP) over the oceans for Jan and Jul 2001. Statistics are binned by region as denoted on the abscissa. The maximum (a) vorticity and (b) wind speed within the cyclonic circulation is overwhelmingly higher in the CCMP analysis.

of the marine atmospheric boundary layer. The wind response to changes in stability is not captured by the neutral satellite surface wind observations and is reflected in Fig. 10 as fluctuations in the wind speed difference along major ocean currents. Other features such as eddies can be observed in Fig. 10a.

Removing the effects of stability from the ECMWF analysis enables other features in the difference fields to be isolated. If we first remove the stability effects from the ECMWF analyses using the bulk parameterization technique (Liu et al. 1979), the magnitude of the wind speed difference is reduced nearly everywhere as expected (Fig. 10b). However, in some areas differences are increased, principally in regions of alongshore currents associated with upwelling and low-lying stratus. In other studies by Wentz and collaborators, SSM/I wind speeds are lower than QuikSCAT by up to 1.0 m s^{-1} in many of these same areas (Fig. 11). However, northwest of Africa, for the Canary Current and associated upwelling, differences are present in Fig. 11 but absent in Fig. 10b. The reason for this is unknown, although this region is not as cloudy as some of the other eastern boundary current regions. These effects are significantly reduced when comparing the TMI wind speeds with QuikSCAT. SSM/I winds are principally retrieved based on information in the 37-GHz channel, whereas TMI winds are principally based on the 11-GHz channel. This suggests that the higher-frequency channel is sensitive to some unaccounted for atmospheric or oceanic condition. Cold upwelling, stability, coastal fog, and low-lying stratus are all suspect, but to date extensive RSS studies have yet to confirm or rule out these hypotheses.

CONCLUSIONS AND FUTURE PLANS. Air–sea interactions are vitally important to the evolution and energetics of weather systems (Atlas 1987) and water masses and thus

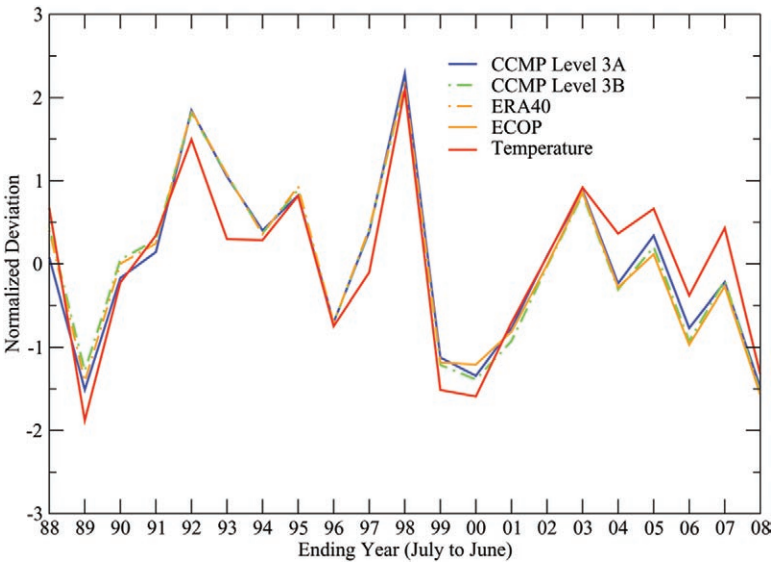

Fig. 8. Time-series plot showing the relationship between the strength of easterly 10-m winds from CCMP 3.5A, CCMP 3.5B, ECOP, and ERA-40 in the central Pacific Niño-4 region and SST anomalies in the eastern Pacific Niño-3.4 region. Cooling (negative SST anomaly) corresponds to stronger easterlies (negative zonal wind) associated with La Niña events, whereas warming episodes correlate with weaker easterlies associated with El Niño events. Values are plotted at the ending year of the annual mean (Jul–Jun).

to ocean circulation and climate-scale atmospheric phenomena such as the ENSO and MJO and persistent anomalies such as heat waves and drought (Wolfson et al. 1987; Atlas et al. 1993). Accurate knowledge of air–sea interactions, including the fluxes of momentum, heat, and mass, depends on accurate knowledge of the ocean surface wind. The CCMP winds described here are an accurate depiction of the winds over the World Ocean (excluding the Arctic Ocean) at high spatial resolution (25 km) and high temporal frequency (every 6 h for more than 20 yr).

To create the CCMP winds, an enhanced variational analysis method (VAM) performs quality control and combines all available RSS cross-calibrated wind data with available conventional ship and buoy data and ECMWF analyses. Differences between the

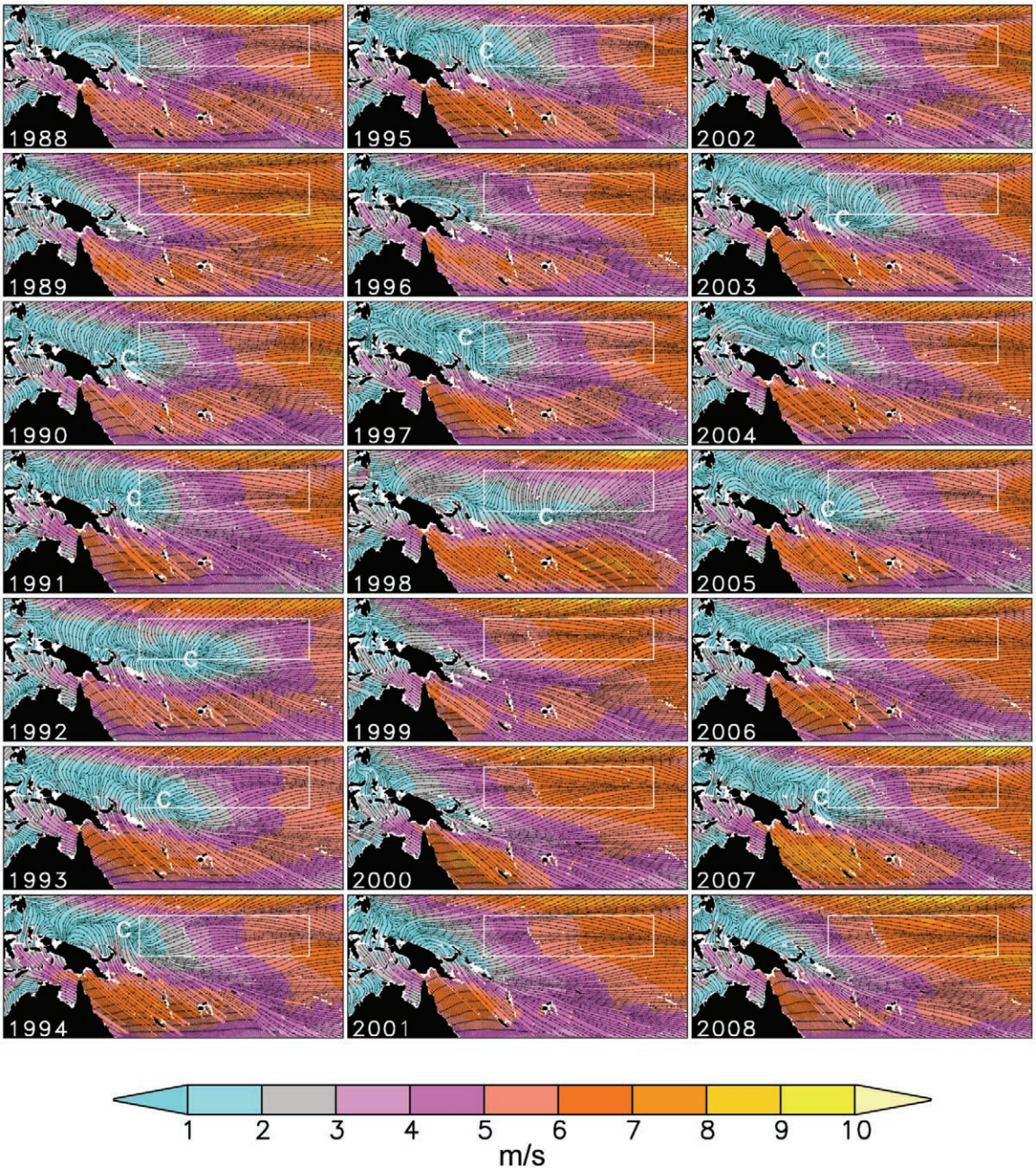

Fig. 9. Annual streamlines and vector magnitude (m s^{-1}) for 21 yr from 1988 to 2008. Means were computed by time averaging the CCMP level-3.0 gridded analyses (*u* and *v*) using only those grid points where satellite surface wind data were analyzed. Each panel represents a time average from July of the previous year to June of the year indicated on the panels. A white rectangle indicates the Niño-4 region. A letter C marks the leading edge of convergence in the 10-m wind field associated with warmer SSTs.

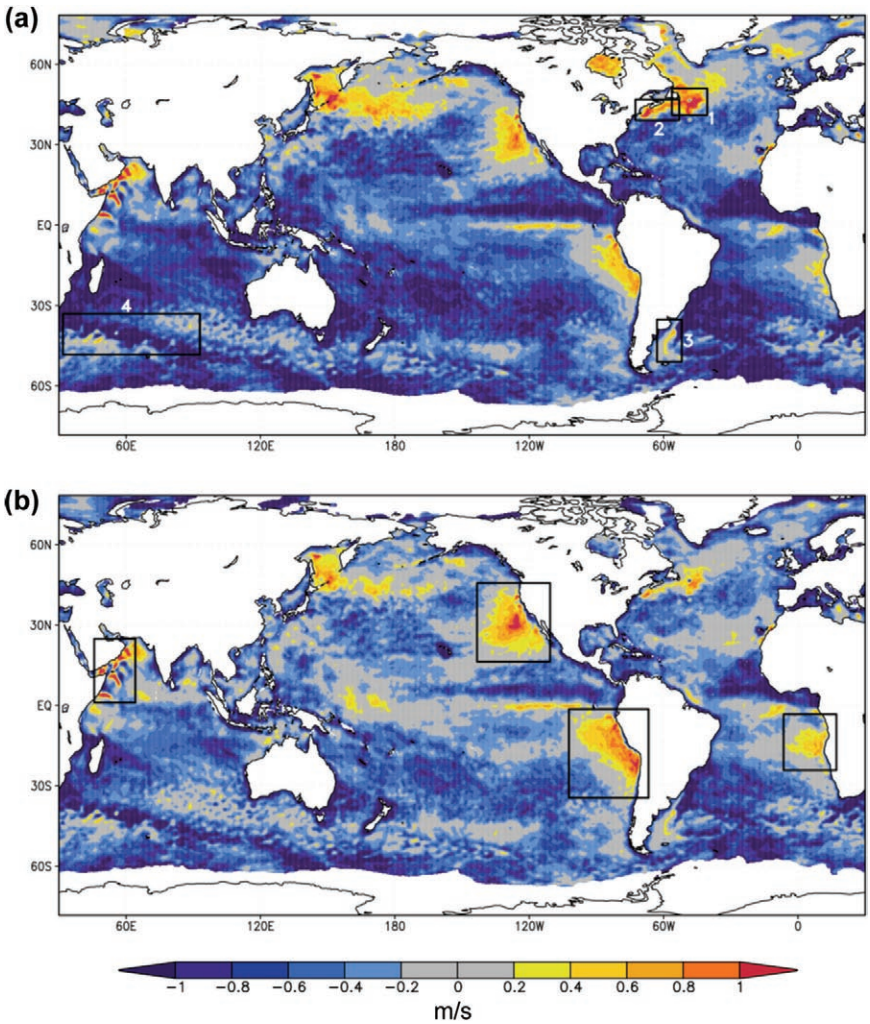

Fig. 10. Mean wind speed difference between the ECMWF and CCMP analysis (ECOP – CCMP) for Jul 2005 with stability effects (a) included in the ECMWF analysis and (b) adjusted to neutral. Stability effects and ocean currents are revealed in the differences. Observable features include 1) the Mann Eddy, 2) the Gulf Stream, 3) the Malvinas Current, and 4) the Agulhas Return Current. Regions highlighted in (b) do not diminish when stability effects are removed from the ECMWF background. Differences in these regions are most likely related to persistent atmospheric or oceanic conditions affecting the microwave remote sensing of the ocean surface.

VAM analyses and wind observations used are small, approximately 0.5 m s^{-1}. VAM analyses agree to approximately 1.0 m s^{-1} with withheld Navy WindSat observations. Compared to other analyses, CCMP winds are significantly different in some synoptic cases, result in different storm statistics, and provide enhanced high-spatial-resolution time averages of ocean surface wind. It is envisioned that the CCMP winds will be extremely useful in diagnostic studies of the atmosphere, in descriptions and evaluations of air–sea processes, for driving regional- and large-scale ocean models, to provide reliable ocean climatologies, and for other meteorological and oceanographic applications. Already, these data have been shown to be useful as boundary forcing for global ocean models (E. Hackert 2007, personal communication).

Currently, the CCMP datasets extend from July 1987 through June

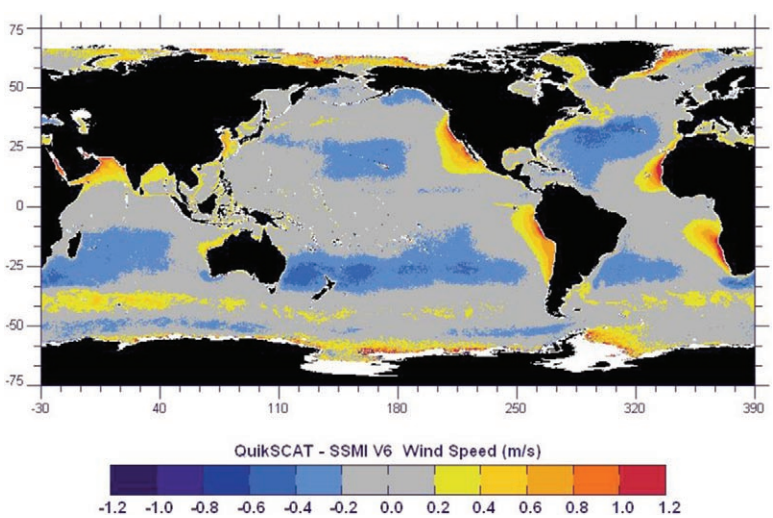

Fig. 11. Mean wind speed difference (QuikSCAT − SSM/I) for the period 1999 to Jun 2009 showing areas of significant differences between the RSS cross-calibrated wind speeds from QuikSCAT and SSM/I. Wind speeds retrieved from TMI (11 GHz) agree more closely with QuikSCAT, indicating that the higher-frequency channel used for SSM/I (37 GHz) is sensitive to certain atmospheric or oceanic conditions that have yet to be identified.

2008. Future plans include extending the dataset at intervals, nominally twice per year, to keep current and incorporating a bias correction to the ECMWF background winds. As ocean wind vector data from additional satellite missions become available from RSS, these data will be added to the VAM inputs, and the affected periods will be reprocessed. Currently, data from three scatterometer instruments and the WindSat radiometer are not available within the RSS cross-calibrated suite of ocean surface winds. The scatterometers are the NASA Scatterometer (NSCAT) and the *ERS-1* and *ERS-2* Active Microwave Instruments (AMIs). The *ERS-1* and *ERS-2* surface wind data are used by ECMWF in both operational analyses and reanalyses. NSCAT provides global coverage for a 9-month period. Here, available WindSat data are used as an independent source of ocean surface wind speed validation data. In the future, as RSS produces new intercalibrated datasets for all available microwave radiometers [including WindSat and Special Sensor Microwave Imager Sounder (SSMIS)] and all C- and Ku-band scatterometers [including the *ERS-1*, *ERS-2*, and Advanced Scatterometer (ASCAT)], we will reprocess the corresponding time periods.

ACKNOWLEDGMENTS. Remote Sensing Systems (RSS; Santa Rosa, California; available online at www.remss.com/) provided the satellite data. We thank F. Wentz of RSS for help in acquiring and understanding these datasets. The conventional data used in our analyses were obtained from the Scientific Division of the National Center for Atmospheric Research (NCAR). Additional buoy data were obtained from the Pacific Marine and Environmental Laboratory (PMEL). ERA-40 Re-Analysis and ECMWF operational analysis datasets were obtained from the Computation and Information Systems Laboratory (CISL) at NCAR. The cross-calibrated multiplatform (CCMP) ocean surface wind product is hosted at the Physical Oceanography Distributed Active Archive Center (PO.DAAC; available online at http://podaac.jpl.nasa.gov/DATA_CATALOG/ccmpinfo.html). We thank D. Moroni (Jet Propulsion Laboratory, California Institute of Technology, Pasadena, California) for help in preparing the CCMP winds for public release. NASA's Research, Education and Applications Solution Network (REASON) and Making Earth Science Data Records for Use in Research Environments (MEASURES) programs funded this work. All of the RSS data described here were produced through another component of the MEASURES program, named the Distributed Information Services: Climate/Ocean Products and Visualizations for Earth Research (DISCOVER) project. The work represents a continuation and expansion of the SSMI Derived Global Ocean Surface Wind Components project that began under the NASA Pathfinder Program. We thank the reviewers and the editor for their useful suggestions that helped to improve this paper.

REFERENCES

Atlas, R., 1987: The role of oceanic fluxes and initial data in the numerical prediction of an intense coastal storm. *Dyn. Atmos. Oceans,* **10,** 359–388.

——, 1997: Atmospheric observations and experiments to assess their usefulness in data assimilation. *J. Meteor. Soc. Japan,* **75,** 111–130.

——, N. Wolfson, and J. Terry, 1993: The effect of SST and soil moisture anomalies on the 1988 U.S. summer drought. *J. Climate,* **6,** 2034–2048.

——, R. N. Hoffman, S. C. Bloom, J. C. Jusem, and J. Ardizzone, 1996: A multiyear global surface wind velocity dataset using SSM/I wind observations. *Bull. Amer. Meteor. Soc.,* **77,** 869–882.

Bentamy, A., H.-L. Ayina, P. Queffeulou, and D. Croize-Fillon, 2007: Improved near real time surface wind resolution over the Mediterranean Sea. *Ocean Sci.,* **3,** 259–271.

Bourlès, B., and Coauthors, 2008: The PIRATA program: History, accomplishments, and future directions. *Bull. Amer. Meteor. Soc.,* **89,** 1111–1125.

Chelton, D. B., and M. H. Freilich, 2005: Scatterometer-based assessment of 10-m wind analyses from the operational ECMWF and NCEP numerical weather prediction models. *Mon. Wea. Rev.,* **133,** 409–428.

——, ——, and S. K. Esbensen, 2000a: Satellite observations of the wind jets off Central America. Part I: Case studies and statistical characteristics. *Mon. Wea. Rev.,* **128,** 1993–2018.

——, ——, and ——, 2000b: Satellite observations of the wind jets off Central America. Part II: Regional relationships and dynamical considerations. *Mon. Wea. Rev.,* **128,** 2019–2043.

——, M. G. Schlax, M. H. Freilich, and R. F. Milliff, 2004: Satellite measurements reveal persistent small-scale features in ocean winds. *Science,* **303,** 978–983.

Courtier, P., and Coauthors, 1998: The ECMWF implementation of three-dimensional variational assimilation (3D-Var). I: Formulation. *Quart. J. Roy. Meteor. Soc.,* **124,** 1783–1807.

Emery, W. J., and R. E. Thomson, 2001: *Data Analysis Methods in Physical Oceanography.* 2nd ed. Elsevier, 638 pp.

Gaiser, P. W., 2004: The WindSat space borne polarimetric microwave radiometer: Sensor description and early orbit performance. *IEEE Trans. Geosci. Remote Sens.,* **42,** 2347–2361.

Gill, A. E., 1980: Some simple solutions for a heat-induced tropical circulation. *Quart. J. Roy. Meteor. Soc.,* **106,** 447–462.

Henderson, J. M., R. N. Hoffman, S. M. Leidner, J. V. Ardizzone, R. Atlas, E. Brin, and J. V. Ardizzone, 2003: A comparison of a two-dimensional variational analysis method and a median filter for NSCAT ambiguity removal. *J. Geophys. Res.,* **108,** 3176, doi:10.1029/2002JC001307.

Hilburn, K. A., and F. J. Wentz, 2008: Intercalibrated passive microwave rain products from the unified microwave ocean retrieval algorithm (UMORA). *J. Appl. Meteor. Climatol.,* **47,** 778–794.

Hoffman, R. N., 1982: SASS wind ambiguity removal by direct minimization. *Mon. Wea. Rev.,* **110,** 434–445.

——, 1984: SASS wind ambiguity removal by direct minimization. Part II: Use of smoothness and dynamical constraints. *Mon. Wea. Rev.,* **112,** 1829–1852.

——, and S. M. Leidner, 2005: An introduction to the near-real-time QuikSCAT data. *Wea. Forecasting,* **20,** 476–493.

——, and ——, 2010: Some characteristics of time interpolation errors for fluid flows. *J. Atmos. Oceanic Technol.,* **27,** 1255–1262.

——, ——, J. M. Henderson, R. Atlas, J. V. Ardizzone, and S. C. Bloom, 2003: A two-dimensional variational analysis method for NSCAT ambiguity removal: Methodology, sensitivity, and tuning. *J. Atmos. Oceanic Technol.,* **20,** 585–605.

Hollinger, J. P., J. L. Pierce, and G. A. Poe, 1990: SSM/I instrument evaluation. *IEEE Trans. Geosci. Remote Sens.,* **28,** 781–790.

Kalnay, E., and Coauthors 1997: Data assimilation in the ocean and in the atmosphere: What should be next. *J. Meteor. Soc. Japan,* **75,** 489–496.

Liu, W. T., K. B. Katsaros, and J. A. Businger, 1979: Bulk parameterization of air–sea exchanges of heat and water vapor including the molecular constraints at the interface. *J. Atmos. Sci.,* **36,** 1722–1735.1979.

McPhaden, M. J., and Coauthors, 1998: The Tropical Ocean-Global Atmosphere observing system: A decade of progress. *J. Geophys. Res.,* **103,** 14 169–14 240.

Meissner, T., and F. Wentz, 2004: The complex dielectric constant of pure and sea water from microwave satellite observations. *IEEE Trans. Geosci. Remote Sens.,* **42,** 1836–1849.

Milliff, R. F., W. G. Large, J. Morzel, G. Danabasoglu, and T. M. Chin, 1999: Ocean general circulation model sensitivity to forcing from scatterometer winds. *J. Geophys. Res.,* **104,** 11 337–11 358.

Smith, C. K., 2006: A statistical approach to WindSat ocean surface wind vector retrievals. *IEEE Geosci. Remote Sens. Lett.,* **3,** 164–168.

Uppala, S. M., and Coauthors, 2005: The ERA-40 Re-Analysis. *Quart. J. Roy. Meteor. Soc.,* **131,** 2961–3012.

Wentz, F. J., 1997: A well-calibrated ocean algorithm for SSM/I. *J. Geophys. Res.,* **102** (C4), 8703–8718.

——, and R. W. Spencer, 1998: SSM/I rain retrievals within a unified all-weather ocean algorithm. *J. Atmos. Sci.,* **55,** 1613–1627.

——, and D. K. Smith, 1999: A model function for the ocean-normalized radar cross section at 14 GHz derived from NSCAT observations. *J. Geophys. Res.,* **104,** 11 499–11 514.

——, L. A. Mattox, and S. Peteherych, 1986: New algorithms for microwave measurements of ocean winds: Applications to *SeaSat* and the Special Sensor Microwave Imager. *J. Geophys. Res.,* **91,** 2289–2307.

——, D. K. Smith, C. A. Mears, and C. L. Gentemann, 2001: Advanced algorithms for QuikScat and SeaWinds/AMSR. *Proc. Int. Geoscience and Remote Sensing Symp. (IGARSS),* Sydney, Australia, IEEE, 1079–1081.

——, K. A. Hilburn, C. A. Mears, and D. K. Smith, 2003: Progress in understanding the effect of rain on Ku-band microwaves and refinement of the Ku-2001 model function. [Available online at www.remss.com/papers/presentations/wentz_OVWST_2003.pdf.]

——, T. Meissner, and D. K. Smith, 2005: Evaluation of microwave scatterometers and radiometers as satellite anemometers. *Proc. Int. Geoscience and Remote Sensing Symp. (IGARSS),* Seoul, Korea, IEEE, 3310–3313.

——, L. Ricciardulli, K. Hilburn, and C. Mears, 2007: How much more rain will global warming bring? *Science,* **317,** 233–235, doi:10.1126/science.1140746.

Wolfson, N., R. Atlas, and Y. C. Sud, 1987: Numerical experiments related to the summer 1980 U.S. heat wave. *Mon. Wea. Rev.,* **115,** 1345–1357.

Zhang, H.-M., J. J. Bates, and R. W. Reynolds, 2006: Assessment of composite global sampling: Sea surface wind speed. *Geophys. Res. Lett.,* **33,** L17714, doi:10.1029/2006GL027086.